




## Possible existence of tristable polarization states in $\text{LiNbO}_3$ under an open-circuit boundary condition

Shaohui Qiu <sup>1</sup>, Liyang Ma <sup>2</sup>, Shi Liu,<sup>2,3,4</sup> and Huaxiang Fu <sup>1</sup>

<sup>1</sup>*Department of Physics, University of Arkansas, Fayetteville, Arkansas 72701, USA*

<sup>2</sup>*School of Science, Westlake University, Hangzhou, Zhejiang 310024, China*

<sup>3</sup>*Institute of Natural Sciences, Westlake Institute for Advanced Study, Hangzhou, Zhejiang 310024, China*

<sup>4</sup>*Key Laboratory for Quantum Materials of Zhejiang Province, Hangzhou Zhejiang 310024, China*



(Received 6 May 2021; revised 9 July 2021; accepted 18 August 2021; published 27 August 2021)

Hyperferroelectricity is an intriguing phenomenon in that electric polarization persists under the open-circuit boundary condition (OCBC). Using first-principles density functional calculations, we investigate the hyperferroelectric properties of  $\text{LiNbO}_3$ , a technologically important ferroelectric solid. We find that (i) the longitudinal-optic  $A_{2u}(\text{LO}_1)$  phonon is soft with imaginary frequency  $96i \text{ cm}^{-1}$  when centrosymmetric  $\text{LiNbO}_3$  is under OCBC, and this soft LO phonon is shown to differ drastically from the corresponding transverse-optic  $A_{2u}(\text{TO}_1)$  phonon. (ii) The  $A_{2u}(\text{LO}_1)$  phonon is able to yield, under OCBC, a free-energy minimum with well depth of  $-9 \text{ meV}$  at a nonzero polarization of  $0.023 \text{ C/m}^2$ , thereby capable of producing hyperferroelectricity. (iii) The origin that  $A_{2u}(\text{LO}_1)$  is capable of inducing HyFE is determined, and it stems from the *extraordinarily small* mode effective charge of this soft LO phonon. This finding also provides a key guiding principle for searching and designing new hyperferroelectrics. (iv) Despite that  $A_{2u}(\text{LO}_1)$  is able to induce HyFE, we find that the ground state of  $\text{LiNbO}_3$  under OCBC is nevertheless not polar, revealing that the existence of a soft LO phonon does not guarantee HyFE. (v) Interestingly, we further show that  $\text{LiNbO}_3$  under OCBC may exhibit unusual tristable polarization states, with two potential wells of depth  $-23 \text{ meV}$  and  $-1.9 \text{ meV}$ , respectively. Besides providing insightful knowledge for understanding HyFE in general, these results reveal that there is rich and interesting hyperferroelectric physics in  $\text{LiNbO}_3$  under OCBC, in particular.

DOI: [10.1103/PhysRevB.104.064112](https://doi.org/10.1103/PhysRevB.104.064112)

### I. INTRODUCTION

Hyperferroelectricity (HyFE), in which an out-of-plane polarization persists in *proper* ferroelectrics (FE) under an open-circuit boundary condition (OCBC) [1–3], is an intriguing phenomenon of fundamental and technological importance. Unlike improper hybrid FEs in which the structural instability is caused by the rotational soft modes at the zone boundary [4–6], the dominating structural instability in proper FEs is caused by the soft phonon at the zone center. When ferroelectricity is present in proper FEs under OCBC, the out-of-plane polarization often generates a strong depolarization field, which tends to eliminate entirely the polarization [7,8]. Ferroelectricity is thus not anticipated to persist in proper FEs under OCBC, which explains why HyFE is interesting and fundamentally important [9]. Furthermore, certain HyFE materials may also exhibit other favorable properties such as negative longitudinal piezoelectric coefficients [10]. HyFE was previously reported to exist in hexagonal ABC-type semiconducting FEs (such as  $\text{LiBeSe}$  and  $\text{LiZnAs}$ ) [1] and in compounds  $\text{LiBO}_3$  (where  $B$  can be V, Nb, Ta, and Os) [3].

Technologically, lack of ferroelectricity under OCBC limits the miniaturization of FE devices and impairs the applications of FE materials [11]. On the other hand, provided that HyFE exists under OCBC, the storage density of FE memories can be increased [12,13], and the efficiency of switching polarization may be improved due to the reduction in coercive field. Furthermore, by heterostructuring HyFEs

with other functional solids such as semiconductors and/or superconductors, the properties of the combined systems may be effectively tuned by utilizing the polarization in HyFEs.

While the mechanism of HyFE remains unsettled, one possible origin is attributed to the small Born effective charge of ions and small longitudinal-optic/transverse-optic splitting [1]. However, Li *et al.* pointed out that this may not be necessary; for instance, HyFE was reported to exist in  $\text{LiBO}_3$ -type materials in which the Born effective charges of ions are large [3]. Other possible explanations include deep internal-energy well and small spontaneous polarization [2], the significance of short-range interaction [3,14], or the existence of meta-screening [15].

Despite the importance of HyFE, many issues of fundamental relevance nevertheless remain not fully understood. (i) First, it is profoundly important to seek reliable methods that can accurately determine whether a solid is HyFE. Currently, one key approach is to use the existence of soft longitudinal-optic (LO) phonon with imaginary frequency as the standard criterion [1–3]. This approach is widely used, and the existence of a soft LO phonon is commonly thought as the hallmark of HyFE. Recently this approach was employed to predict that  $\text{LiBO}_3$  is HyFE [3]. Nevertheless, one critical question remains unanswered: is this hallmark of HyFE fully justified? Is it possible that a solid possessing soft LO phonon may turn out to be *not* a HyFE? (ii) It remains fundamentally interesting and meanwhile elusive to understand why the

strong depolarization field does not eliminate the polarization in HyFE and what physical origin leads to its nonzero polarization under OCBC. Discovery of this origin may vastly expand our understanding of HyFE. (iii) In the search for new HyFEs, we often rely on the trial-and-error approach, which is time-consuming and less efficient. In light of this, one may wonder whether there exists any pivotal physical quantity that is of unique importance in terms of providing the much-needed guide in the designing and searching for new HyFEs. (iv) Are there any interesting and previously-unknown phenomena, which wait to be discovered in HyFEs?

The purpose of this paper is to address the above subjects of fundamental relevance. Instead of using the existence of soft LO phonon as the criterion of determining HyFE [3], we here use a different (and more rigorous) approach by determining the electric free energy under OCBC. The approach of electric free energy is powerful and generally applicable because, provided that a solid is HyFE, it should by definition exhibit a nonzero polarization at the minimum of free energy when the solid is under OCBC. We choose to consider LiNbO<sub>3</sub> since this material is technologically important by possessing strong ferroelectricity and piezoelectricity, high electro-optic coefficient, and photoelastic effect [16]. In fact, LiNbO<sub>3</sub> has been widely used in optical parametric oscillators, beam deflectors, memory elements, electro-optic and nonlinear optical devices [16]. The LiNbO<sub>3</sub> solid belongs to the R3c space group in FE phase and the R $\bar{3}$ c space group in PE phase. The PE-to-FE phase transition occurs at 1480 K.

Driven by the technological interest, various properties of LiNbO<sub>3</sub> have been studied previously. For example, neutron scattering shows evidence that the phase transition in LiNbO<sub>3</sub> is largely order-disorder type [17]. The fundamental band gap of LiNbO<sub>3</sub> was calculated using GW approach and Bethe-Salpeter equation, along with the phonon frequencies in FE and PE LiNbO<sub>3</sub> [18]. In particular, the frequencies of the soft A<sub>2u</sub> and A<sub>2g</sub> modes were found to be 183i and 92i cm<sup>-1</sup>, respectively [18]. Raman scattering efficiency were calculated and assigned to the measured Raman peaks [19], and the theory confirms the experimental results [20]. By using the vibration free energy, the FE-to-PE Curie temperature was theoretically determined [21]. Furthermore, localized vibration modes were found to exist both at the positive and negative surfaces of LiNbO<sub>3</sub> [22].

Besides addressing the key issues on HyFE as described above, we will further answer some critical questions regarding LiNbO<sub>3</sub>. These questions include (1) whether LiNbO<sub>3</sub> is HyFE under OCBC? (2) How deep is the HyFE potential well, if HyFE exists in LiNbO<sub>3</sub>? (3) How large is the hyperferroelectric polarization when LiNbO<sub>3</sub> is under OCBC? These questions cannot be (and have not been) rigorously addressed in previous study, which uses the approach of predicting HyFE according to the existence of soft LO phonon [3].

We find that (i) the longitudinal A<sub>2u</sub>(LO<sub>1</sub>) soft mode at imaginary frequency 96i cm<sup>-1</sup> in LiNbO<sub>3</sub> yields, under OCBC, a nonzero polarization of magnitude P = 0.023 C/m<sup>2</sup>. The physical origin responsible for the existence of this nonzero polarization, despite that the system is under OCBC, is found to stem from the remarkably small depolarization energy caused by the A<sub>2u</sub>(LO<sub>1</sub>) phonon, which is about *three orders of magnitude* smaller than the depolarization energy

caused by the corresponding transverse-optic (TO) phonon. (ii) However, and interestingly, we discover that the *ground state* of LiNbO<sub>3</sub> under OCBC is nevertheless *not* hyperferroelectric, which differs from previous study where LiNbO<sub>3</sub> was concluded to be HyFE [3]. Instead we find that the ground state of LiNbO<sub>3</sub> under OCBC is nonpolar. This important finding reveals that possessing a soft LO mode does not guarantee that the solid is HyFE. Therefore, one must be cautious when using the hallmark criterion of determining HyFE according to the soft LO mode. (iii) The reason that the ground state of LiNbO<sub>3</sub> is not HyFE can be attributed to the fact that there is a strong nonpolar mode, being soft at frequency 120i cm<sup>-1</sup> under OCBC, and this mode drives the system to be nonpolar. (iv) Moreover, we reveal another intriguing phenomenon, namely that LiNbO<sub>3</sub> under OCBC may possess an unusual, triple potential well. In other words, LiNbO<sub>3</sub> under OCBC exhibits three stable and/or metastable states with different polarizations.

## II. THEORETICAL METHODS

A combination of three different methods is used to investigate the hyperferroelectric properties in LiNbO<sub>3</sub>. (i) We use the first-principles linear response theory [23–26] to determine the phonon eigenvalues and eigenvectors, paying particular attention to the TO and LO phonons. The appearance of soft TO phonon gives rise to structural instability under the short-circuit boundary condition (SCBC). Meanwhile, the existence of soft LO phonon indicates the possibility of structural instability under OCBC, since an LO phonon is obtained after the corresponding (one or multiple) TO phonons interact with the macroscopic electric field induced by lattice vibration [27–29]. (ii) To determine the magnitude of electric polarization in the system, we use the modern theory of polarization via the geometric Berry-phase approach [30,31]. (iii) We determine whether a solid is HyFE by optimizing the electric free energy under OCBC [32]. When a solid under OCBC exhibits a nonzero polarization at the free-energy minimum, HyFE occurs. These methods are described in the following.

### A. Linear-response phonon calculations

Phonon calculations are performed using the density functional perturbation theory (DFPT) [23–26]. Change in bare-ions potential  $\Delta V$  due to atomic vibration is treated as perturbation, and the response of electron state  $|\Delta\psi_n\rangle$  is obtained by solving the Sternheimer equation [23],

$$(H_{scf} - \varepsilon_n) |\Delta\psi_n\rangle = -(\Delta V_{scf} - \Delta\varepsilon_n) |\psi_n\rangle, \quad (1)$$

where  $H_{scf}$  is the single-particle Kohn-Sham Hamiltonian,  $\varepsilon_n$  is the eigenvalue of  $H_{scf}$ ,  $\Delta V_{scf}(\mathbf{r}) = \Delta V(\mathbf{r}) + e \int \frac{\Delta\rho(\mathbf{r}')}{|\mathbf{r}-\mathbf{r}'|} d\mathbf{r}' + \frac{dv_{xc}(\rho)}{d\rho}|_{\rho=\rho(\mathbf{r})} \Delta\rho(\mathbf{r})$  is the first-order correction to the self-consistent  $V_{scf}(\mathbf{r})$  potential, and  $\Delta\varepsilon_n = \langle\psi_n|\Delta V_{scf}(\mathbf{r})|\psi_n\rangle$  is the first-order correction to eigenvalue  $\varepsilon_n$ . Born effective-charge tensor ( $Z$ ) and high-frequency dielectric tensor ( $\epsilon_\infty$ ) are also determined within the DFPT calculations.

Phonon frequencies and eigenvectors are obtained by solving the secular equation  $\det|\frac{1}{\sqrt{M_i M_j}} C_{\alpha, j\beta}(\vec{q}) - \omega^2(\vec{q})| = 0$ , where  $C(\vec{q})$  is the force-constant matrix,  $\omega$  is frequency,  $i$

and  $j$  are atomic indices, and  $\alpha$  and  $\beta$  are the Cartesian-direction indices [33].  $C(\vec{q})$  includes both analytic  $C^a$  and nonanalytic  $C^{na}$  contributions [25]. The analytic part  $C^a$  is the force-constant matrix computed directly from DFPT under zero macroscopic electric field. The nonanalytic part  $C^{na}$  is caused by the fact that, in the long-wavelength limit  $q \rightarrow 0$ , an LO phonon leads to a macroscopic electric field, which is to interact with the lattice vibration. The nonanalytic term is given as  $C_{\alpha\alpha, j\beta}^{na}(\vec{q}) = \frac{4\pi}{\Omega} e^{2\frac{(\vec{q}\cdot Z_i)_\alpha(\vec{q}\cdot Z_j)_\beta}{\vec{q}\cdot\epsilon_\infty\vec{q}}}$ , where  $Z_i$  is the Born effective-charge tensor of atom  $i$  and  $\epsilon_\infty$  is the high-frequency dielectric tensor due to the electron response [25].

It should be pointed out that, when  $C^{na}$  is not included in the dynamic matrix, there is no macroscopic electric field in the solid (which corresponds to the electrical boundary condition of SCBC), and the existence of soft modes (if any) thus indicates the structure instability under SCBC [26]. On the other hand, when  $C^{na}$  is included in the dynamic matrix, the macroscopic electric field is nonzero (which corresponds to the electrical boundary condition of OCBC), and the existence of soft modes indicates the structure instability under OCBC.

### B. Polarization calculations

Electric polarization consists of ionic and electronic contributions. Ionic contribution can be calculated directly using point charges as  $\vec{P}_{\text{ion}} = \frac{1}{\Omega} \sum_i q_i \vec{r}_i$ , where  $q_i$  is the charge of ion  $i$  and  $\vec{r}_i$  is the ion position. Electronic contribution is calculated using the modern theory of polarization via the Berry-phase approach [30,31],

$$\vec{P}_{\text{el}} = \frac{2e}{(2\pi)^3} \int d\vec{k}_\perp \text{Im} \ln \prod_j \det(\langle u_{m, \vec{k}_\parallel} | u_{n, \vec{k}_\parallel + \vec{j}} \rangle), \quad (2)$$

where  $u_{n\vec{k}}$  is the cell-periodic Bloch part of occupied wave functions,  $\vec{k}_\perp$  and  $\vec{k}_\parallel$  are, respectively, the components of the electron wave vector perpendicular and parallel to the polarization direction. Microscopic understanding of  $\vec{P}_{\text{el}}$  from individual  $\vec{k}_\perp$  string can be further analyzed using the theory of polarization structure [34].

### C. Electric free energy under OCBC

When a FE solid is under OCBC (i.e., with a vanishing electric displacement  $D = 0$ ), a macroscopic electric field  $E$  is to appear, which will interact with polarization and polarize the electron wave functions. To make our theory generally applicable, we consider an arbitrary atomic configuration  $\{\vec{r}_i(\lambda)\}$  parametrized by  $\lambda$ . Here,  $\{\vec{r}_i(\lambda)\}$  can be an intermediate configuration between the centrosymmetric configuration  $\{\vec{r}_i^c\}$  of the paraelectric (PE) phase and the ferroelectric configuration  $\{\vec{r}_i^f\}$  of the FE phase, according to  $\vec{r}_i(\lambda) = \vec{r}_i^c + \lambda(\vec{r}_i^f - \vec{r}_i^c)$ , where  $i$  is the atomic index and  $\lambda$  is the control parameter by which we vary the atomic configuration. Alternatively, the configuration  $\{\vec{r}_i(\lambda)\}$  can be obtained by shifting the atoms in the PE phase according to the eigendisplacement  $|\vec{u}_i\rangle$  of a given phonon mode as

$$\vec{r}_i(\lambda) = \vec{r}_i^c + \lambda a_0 \vec{u}_i, \quad (3)$$

where  $a_0$  is the lattice constant. For configuration  $\lambda$ , the electric free energy under OCBC is [35]

$$F(\lambda) = U(\lambda) - \Omega(\lambda)[P(\lambda) \cdot E + \frac{1}{2}\epsilon_0\chi_\infty(\lambda)E^2], \quad (4)$$

which  $U(\lambda)$ ,  $\Omega(\lambda)$ ,  $P(\lambda)$ , and  $\chi_\infty(\lambda) = \epsilon_\infty(\lambda) - 1$  are, respectively, the internal energy, unit-cell volume, electric polarization, and the  $\chi_\infty^{33}$  component of high-frequency dielectric permittivity at configuration  $\lambda$ ; all these quantities are computed from the DFT calculations at zero macroscopic electric field because Eq. (4) is essentially a second-order Taylor expansion of the free energy around the zero field [32]. Since we are interested in the circumstances where the electric field is along the direction of polarization, the vector notations are thus dropped in Eq. (4). For a given  $E$  field, the total electric polarization is obtained from Eq. (4) as  $P_{\text{tot}} = -\frac{1}{\Omega} \frac{\partial F}{\partial E} = P(\lambda) + \epsilon_0\chi_\infty(\lambda)E$ , and the electric displacement is  $D(\lambda) = \epsilon_0E + P_{\text{tot}} = P(\lambda) + \epsilon_0[1 + \chi_\infty(\lambda)]E$ . Under OCBC where  $D$  vanishes, the macroscopic  $E$  field is thus

$$E = -\frac{P(\lambda)}{\epsilon_0[1 + \chi_\infty(\lambda)]}. \quad (5)$$

Combining Eq.(4) and Eq.(5), the free energy of arbitrary configuration  $\lambda$  under OCBC is [32]

$$F = U(\lambda) + \Omega(\lambda) \frac{1 + \frac{1}{2}\chi_\infty(\lambda)}{\epsilon_0[1 + \chi_\infty(\lambda)]^2} P^2(\lambda), \quad (6)$$

where all quantities on the right-hand side can be computed by DFT. The second term in Eq. (6) is clearly the energy cost introduced by the depolarization field under OCBC, and will be denoted as

$$U_{\text{dp}} = \Omega(\lambda) \frac{1 + \frac{1}{2}\chi_\infty(\lambda)}{\epsilon_0[1 + \chi_\infty(\lambda)]^2} P^2(\lambda). \quad (7)$$

If the free energy under OCBC exhibits a global minimum at a configuration with nonzero polarization, the solid is then a HyFE.

### D. Computational details

Technically we use the density functional theory (DFT) within the local density approximation (LDA) to calculate the total (internal) energy and atomic forces, and to optimize the structure. Computations are performed using QUANTUM ESPRESSO [36,37]. Troullier-Martins type of norm-conserving pseudopotentials is generated to replace the effects of core electrons [38]. The rhombohedral unit cell of LiNbO<sub>3</sub> with ten atoms is used. The cutoff energy for plane-wave expansion of the single-particle wavefunctions is 110 Ry, which is sufficient.

The LiNbO<sub>3</sub> crystal can be described either using a 10-atoms rhombohedral unit cell with lattice constant  $a_R$  and angle  $\gamma$  between two trigonal lattice vectors [Fig. 1(a)], or using a 30-atoms hexagonal unit cell with in-plane lattice constant  $a_H$  and out-of-plane lattice constant  $c$  [Fig. 1(b)]. The relationship between the lattice parameters of these two cells is:  $a_R = \frac{1}{3}\sqrt{3a_H^2 + c^2}$  and  $\sin \frac{\gamma}{2} = \frac{3/2}{\sqrt{3+c^2/a_H^2}}$ . For the FE phase of bulk LiNbO<sub>3</sub> under SCBC, our structural optimization yields  $a_R = 5.444 \text{ \AA}$  and  $\gamma = 55.813^\circ$ , which are close to experimental results  $a_R = 5.494 \text{ \AA}$  and  $\gamma = 55.867^\circ$  [39]. The electric polarization in FE LiNbO<sub>3</sub> is calculated to be

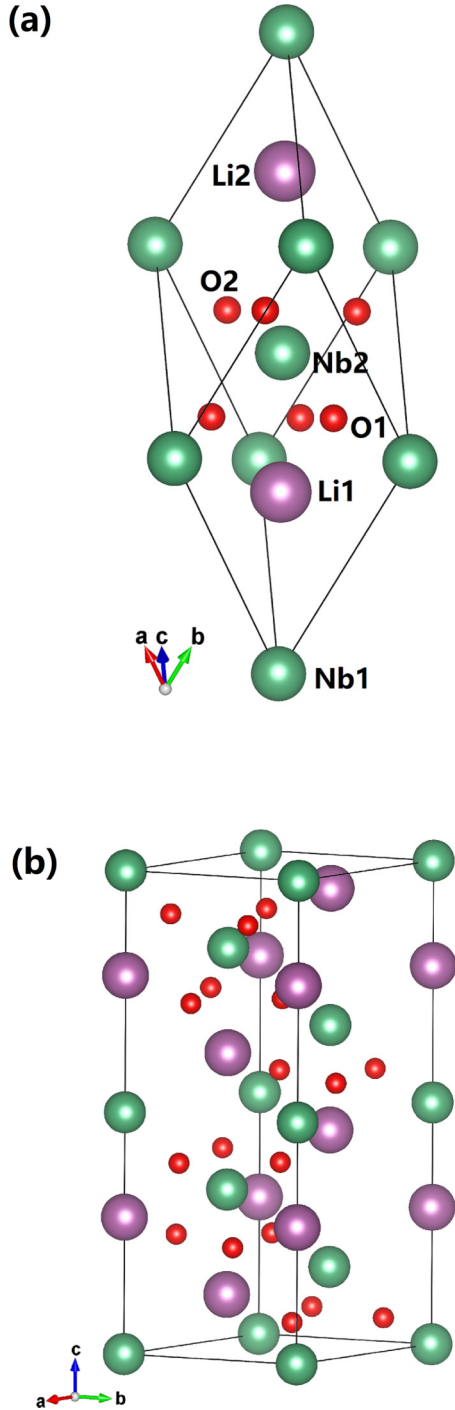


FIG. 1. Crystal structure of LiNbO<sub>3</sub>: (a) 10-atom rhombohedral unit cell, (b) 30-atom hexagonal unit cell. Li, Nb, and O atoms are shown in purple, green, and red spheres, respectively.

0.768 C/m<sup>2</sup>, agreeing with the experimental value of 0.71 C/m<sup>2</sup> [40]. The depth of the FE double potential wells is determined to be  $-258$  meV, close to the value of  $-259$  meV in another study [41].

To examine the hyperferroelectric properties, we also need to consider the PE phase since HyFE occurs often near the PE phase. For PE LiNbO<sub>3</sub> with centrosymmetry, atoms are located at Li (0.25, 0.25, 0.25), Nb (0, 0, 0), and O ( $u$ , 0.5 –

TABLE I. The zone-center phonon modes of key relevance (2nd column), frequency  $\omega$  (3rd column), and mode-specific effective charge  $\tilde{Z}_3^{nq}$  (4th column) in centrosymmetric LiNbO<sub>3</sub>. Results calculated without (and with) nonanalytic  $C^{na}$  contribution in dynamic matrix are given in the upper (and lower) part of the Table. The nonsoft A<sub>2u</sub>(TO<sub>2</sub>) mode is also listed since it participates in forming the A<sub>2u</sub>(LO<sub>1</sub>) mode.

$C^{na}$ or not	Modes	$\omega$ (cm <sup>-1</sup> )	$\tilde{Z}_3^{nq}$
without $C^{na}$	A <sub>2u</sub> (TO <sub>1</sub> )	202 <i>i</i>	6.65
	A <sub>2g</sub>	113 <i>i</i>	0.00
	A <sub>2u</sub> (TO <sub>2</sub> )	95	-4.21
with $C^{na}$	A <sub>2g</sub>	120 <i>i</i>	0.00
	A <sub>2u</sub> (LO <sub>1</sub> )	96 <i>i</i>	0.39

$u$ , 0.75) in the coordinate frame of the rhombohedral lattice vectors. We optimize both the cell parameters and internal parameter  $u$  while constraining the R $\bar{3}c$  symmetry, and we obtain  $a_R = 5.394$  Å,  $\gamma = 56.7^\circ$ , and  $u = 0.1275$ . Converting our theoretical results from the rhombohedral cell to the hexagonal cell, we find  $a_H = 5.1228$  Å,  $c = 13.5326$  Å, and an O-atom position ( $0.0441, \frac{1}{3}, \frac{1}{12}$ ). These values agree well with  $a_H = 5.1378$  Å,  $c = 13.4987$  Å, and the O atom position ( $0.0490, \frac{1}{3}, \frac{1}{12}$ ) in Ref. [42], and with  $a_H = 5.1250$  Å,  $c = 13.5480$  Å, and the O atom position ( $0.0420, \frac{1}{3}, \frac{1}{12}$ ) in Ref. [43]. In PE LiNbO<sub>3</sub>, our calculated  $Z_{33}^*$  effective charges are 1.11, 9.03, and  $-3.36$ , respectively, for Li, Nb, and O atoms, which are close to the values of 1.11, 9.17, and  $-3.43$  in another calculation [43]. All results show that our calculations are rather reliable.

### III. RESULTS AND DISCUSSIONS

#### A. LO phonon in LiNbO<sub>3</sub>

Since HyFE is closely connected with LO phonon, we begin by presenting the LO phonon in PE LiNbO<sub>3</sub>. Table I lists the calculated phonon frequencies for several zone-center modes of key importance in PE LiNbO<sub>3</sub>, obtained from the linear response calculations. Note that we report in Table I the phonon frequencies, calculated both *with* and *without* the nonanalytical  $C^{na}$  contribution in the dynamic matrix.

Table I reveals that (i) when  $C^{na}$  is not included (i.e., under SCBC), there are two soft modes, one is the A<sub>2u</sub>(TO<sub>1</sub>) mode at frequency  $\omega = 202i$  cm<sup>-1</sup> and the other is the nonpolar A<sub>2g</sub> mode at  $\omega = 113i$  cm<sup>-1</sup> (see the upper part of Table I) [44]; (ii) When  $C^{na}$  is included (i.e., when macroscopic electric field is nonzero), the A<sub>2g</sub> mode remains to be soft, and its frequency barely changes from  $113i$  cm<sup>-1</sup> to  $120i$  cm<sup>-1</sup> (see the lower part of Table I). This is not surprising since the A<sub>2g</sub> mode is nonpolar and thus does not interact strongly with the macroscopic electric field. (iii) Interestingly, besides *nonpolar* A<sub>2g</sub>, another *polar* mode remains soft after  $C^{na}$  is included, that is, the longitudinal-optic A<sub>2u</sub>(LO<sub>1</sub>) mode. Furthermore, the frequency of A<sub>2u</sub>(LO<sub>1</sub>) is rather strongly imaginary at  $\omega = 96i$  cm<sup>-1</sup>, suggesting that this mode is to cause a significant structure instability under OCBC.

To provide microscopic insight into the structure instability, we show in Fig. 2 the phonon eigenvectors of those modes

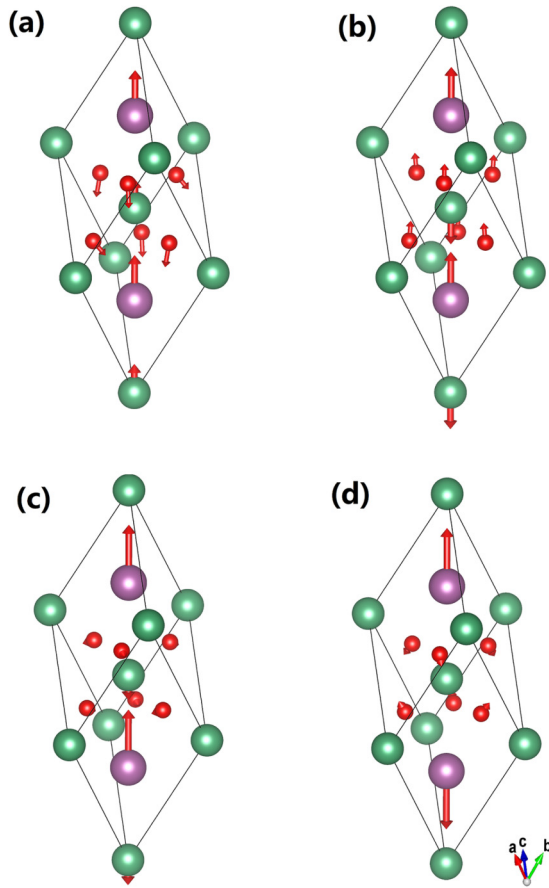


FIG. 2. Phonon eigenvectors for the following modes: (a)  $A_{2u}(TO_1)$ , (b)  $A_{2u}(TO_2)$ , (c)  $A_{2u}(LO_1)$ , (d) nonpolar  $A_{2g}$ . Li, Nb, and O atoms are shown in purple, green, and red spheres, respectively, as in Fig. 1(a).

in Table I. For  $A_{2u}(TO_1)$  in Fig. 2(a), we see that positively-charged Li and Nb ions move along the same direction, and negatively-charged O ions move in an opposite direction along the polar axis, showing that  $A_{2u}(TO_1)$  is a polar mode. For  $A_{2u}(TO_2)$ , which is *not* soft, Fig. 2(b) tells that, while Nb and O atoms move along opposite directions, Li and O atoms nevertheless move along the same direction. The soft LO phonon of  $A_{2u}(LO_1)$  in Fig. 2(c) is more intriguing—this mode consists predominantly of the displacements of Li atoms, with small but not negligible contributions from Nb and O atoms. The  $A_{2g}$  mode in Fig. 2(d) reveals that two Li atoms move along opposite directions with the same magnitude (which maintains the centrosymmetry), and therefore this mode is indeed nonpolar.

Since soft LO phonon plays a pivotal role in developing HyFE, we go one step further and attempt to find out where  $A_{2u}(LO_1)$  originates from, by performing the following mode analysis [29]. Let us use the ket vector  $|\omega_i\rangle$  to denote the phonon eigenvectors obtained from the dynamic matrix *without* the nonanalytic  $C^{na}$  contribution, and use  $|\omega'_i\rangle$  to denote the eigenvectors obtained from the dynamic matrix *with* the  $C^{na}$  contribution. We recognize that the eigenvectors  $|\omega_i\rangle$  at the  $\vec{q} = 0$  zone center form a complete basis set for this phonon wave vector. We can thus use  $|\omega_i\rangle$  as bases and

expand  $|\omega'_i\rangle$  according to  $|\omega'_j\rangle = \sum_i t_{ij} |\omega_i\rangle$ , where coefficients  $t_{ij} = \langle \omega_i | \omega'_j \rangle$  should tell us quantitatively which modes participate in forming a given  $|\omega'_j\rangle$  mode. We find that  $|A_{2u}(LO_1)\rangle = \sqrt{0.39}|A_{2u}(TO_1)\rangle + \sqrt{0.61}|A_{2u}(TO_2)\rangle$ . It reveals two important outcomes: (i)  $A_{2u}(LO_1)$  and  $A_{2u}(TO_1)$  do not have the same eigenvectors, and instead  $A_{2u}(TO_1)$  contributes only 39% in the process of forming  $A_{2u}(LO_1)$ . This is in marked difference with semiconductor ZnO where LO and TO modes have nearly identical eigenvectors although their frequencies differ [32]. (ii)  $A_{2u}(LO_1)$  mainly comes from the nonsoft  $A_{2u}(TO_2)$ , which suggests a critical knowledge that *nonsoft* phonon may play an important role in forming HyFE.

### B. Can soft $A_{2u}(LO_1)$ yield HyFE?

After finding that  $A_{2u}(LO_1)$  is soft, it then becomes interesting to investigate (i) how strong a (HyFE) spontaneous polarization may be induced by this longitudinal mode, and (ii) how deep the HyFE potential well will be under OCBC. These questions are nontrivial particularly when system is under OCBC, and the answers are previously unknown. For this purpose, we calculate the electric free energies along the configuration path as parameterized in Eq. (3) by using the vibration eigendisplacement  $|\vec{u}_i\rangle$  of  $A_{2u}(LO_1)$ .

The calculated free energy  $F(\lambda)$ , along with the internal energy  $U(\lambda)$ , is shown in Fig. 3(a) for LiNbO<sub>3</sub> under OCBC. Fig. 3(a) reveals that, as  $\lambda$  deviates from the PE phase of  $\lambda = 0$ , free energy  $F(\lambda)$  starts to decrease, showing that, under OCBC, the PE phase is unstable against the phonon displacement of the  $A_{2u}(LO_1)$  mode. In other words, we find that the soft  $A_{2u}(LO_1)$  mode can induce, under OCBC, hyperferroelectricity at nonzero  $\lambda$ . Furthermore, our calculations in Fig. 3(a) predict that  $F(\lambda)$  reaches its minimum at  $\lambda = 0.0765$ . We denote the structure phase with a nonzero polarization at  $\lambda = 0.0765$  as the LO-induced HyFE phase.

We further calculate the polarization of the LO-induced HyFE phase using the modern theory of polarization, and find that the polarization is  $P_{LO} = 0.023$  C/m<sup>2</sup>. This polarization is not small and is comparable in magnitude to the value of 0.02 C/m<sup>2</sup> previously found in the ABC-type hyperferroelectric materials LiBeSb and LiZnAs [1]. Furthermore, Fig. 3(a) shows that the free-energy depth of the HyFE potential well is  $\Delta F = -9$  meV, which is close to the internal-energy depth ( $-9.57$  meV) of the double potential well in prototypical ferroelectric BaTiO<sub>3</sub> under SCBC [45]. This is rather remarkable and implies that the Curie temperature of HyFE in LiNbO<sub>3</sub> under OCBC could be as high as that of bulk BaTiO<sub>3</sub> (120°C).

Having seen that  $A_{2u}(LO_1)$  is able to induce a HyFE phase, readers may wonder whether  $A_{2u}(TO_1)$ , the TO mode, can produce a nonzero polarization under OCBC. Here we go one step further and determine the free energy  $F(\lambda)$  under OCBC and the internal energy  $U(\lambda)$  for this TO mode using the  $A_{2u}(TO_1)$  eigendisplacement. The results are shown in Fig. 3(b).

Let us first focus on the internal energy  $U(\lambda)$  in Fig. 3(b). Note in Eq. (4) that, when macroscopic electric field  $E$  vanishes (i.e., when system is under SCBC), the internal energy  $U(\lambda)$  is the free energy, namely  $U(\lambda)$  yields the energetics and

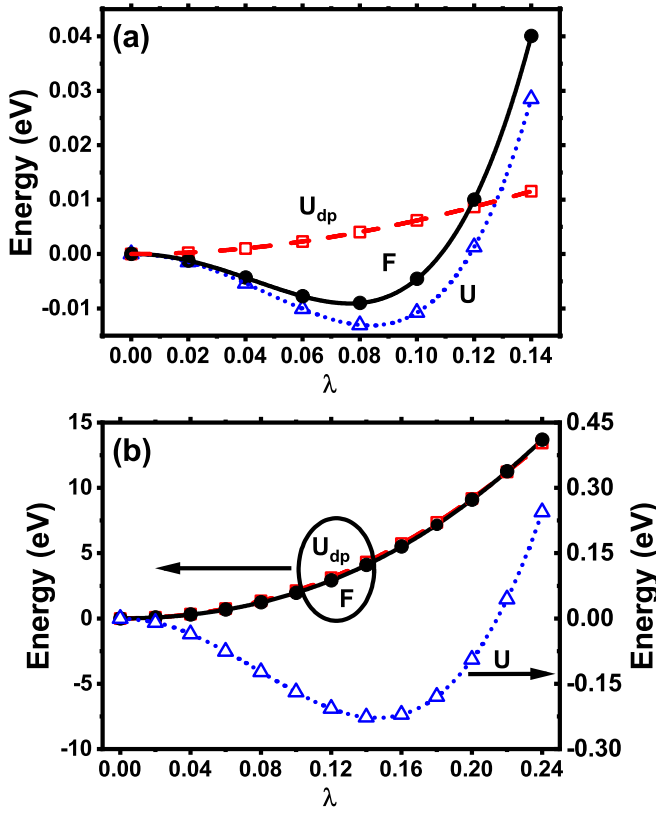


FIG. 3. Electric free energy  $F(\lambda)$  (solid dots), internal energy  $U(\lambda)$  (empty triangles), and depolarization energy  $U_{dp}(\lambda)$  (empty squares) in  $\text{LiNbO}_3$  under OCBC as a function of  $\lambda$ , for the following phonon modes: (a) soft longitudinal  $A_{2u}(\text{LO}_1)$  mode, and (b) soft transverse  $A_{2u}(\text{TO}_1)$  mode. In (b),  $F(\lambda)$  and  $U_{dp}(\lambda)$  are plotted using the left vertical axis, while  $U(\lambda)$  is plotted using the right vertical axis so that the depth of the potential well of  $U(\lambda)$  can be clearly displayed.  $\lambda = 0$  corresponds to the PE phase.  $F(\lambda)$  exhibits a minimum at  $\lambda = 0.0765$  for  $A_{2u}(\text{LO}_1)$  mode in (a).  $U(\lambda)$  exhibits a minimum at  $\lambda = 0.1460$  for  $A_{2u}(\text{TO}_1)$  mode in (b).

structural instability under SCBC. Fig. 3(b) reveals that (i) as  $\lambda$  deviates from  $\lambda = 0$ ,  $U(\lambda)$  drastically decreases and exhibits a minimum at  $\lambda = 0.1460$ . We name the atomic configuration corresponding to this  $\lambda$  value as the TO-induced phase (under SCBC). (ii) The potential well of  $U(\lambda)$  for this TO-induced phase is very deep and is  $-227$  meV [see the triangle symbols and the right vertical axis in Fig. 3(b)]. (iii) We further find that the  $A_{2u}(\text{TO}_1)$  mode is the mode responsible for the FE phase in bulk  $\text{LiNbO}_3$  under SCBC (not OCBC). As a matter of fact, we compute the polarization for the TO-induced phase, and find that the polarization is  $0.756$  C/m<sup>2</sup>, which is very close to the calculated polarization value of  $0.768$  C/m<sup>2</sup> in bulk  $\text{LiNbO}_3$  under SCBC. Furthermore, we examine the atomic off-center displacement  $\Delta r_z$  along the polar  $z$  direction in the TO-induced phase with respect to the centrosymmetric configuration, by fixing one Nb atom at the origin as the reference.  $\Delta r_z$  is defined as  $\Delta r_z(i) = r_z(i) - r_z^c(i)$ , where  $r_z(i)$  and  $r_z^c(i)$  are the  $z$  position of atom  $i$  in the noncentrosymmetric and centrosymmetric phases, respectively.  $\Delta r_z$  is shown in Fig. 4, and we find that the  $\Delta r_z$  values for the TO-induced phase (yellow bars in Fig. 4) and for the bulk FE phase (shaded

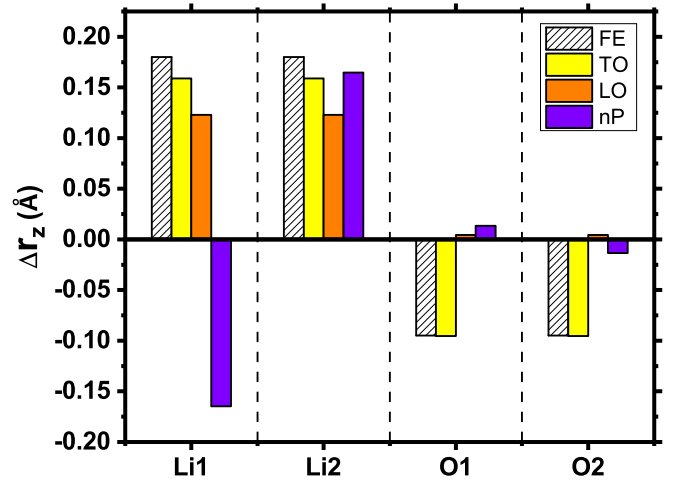


FIG. 4. Atomic off-center displacement  $\Delta r_z$  with respect to the centrosymmetric PE phase, for the following configurations in  $\text{LiNbO}_3$ : the bulk FE phase under SCBC (shaded), the TO-induced phase under SCBC (yellow), the LO-induced phase under OCBC (orange), and the nonpolar nP phase under OCBC (violet). In all cases, one Nb atom is placed at the origin as the reference. Li1 and O1 are located at the bottom of the cell, while Li2 and O2 are located at the top of the cell [see Fig. 1(a)].

bars in Fig. 4) are very close to each other for all atoms, confirming that the  $A_{2u}(\text{TO}_1)$  mode is indeed responsible for the ferroelectricity in bulk  $\text{LiNbO}_3$  under SCBC.

Interestingly, Fig. 3(b) also reveals that, although  $U(\lambda)$  produces a deep internal-energy potential well, the free energy  $F(\lambda)$  nevertheless does not exhibit a minimum at nonzero  $\lambda$  under OCBC. Instead, as  $\lambda$  deviates from  $\lambda = 0$  in Fig. 3(b),  $F(\lambda)$  monotonously increases. Therefore, under OCBC,  $A_{2u}(\text{TO}_1)$  produces only a stable PE phase at  $\lambda = 0$ . This demonstrates that the  $A_{2u}(\text{TO}_1)$  mode cannot generate HyFE under OCBC.

### C. Origin of LO-induced HyFE in $\text{LiNbO}_3$

The finding that the  $A_{2u}(\text{LO}_1)$  mode is able to generate a free-energy minimum at nonzero  $\lambda$  (and thus produce HyFE) under OCBC, despite the fact that the internal-energy well of this soft LO mode is very shallow, is intriguing. We now attempt to provide the physical origin, which aims at understanding why the HyFE free-energy minimum exists.

Figures 5(a)–5(d) shows the computed internal energy  $U$ , electric polarization  $P$ , high-frequency dielectric constant  $\varepsilon_\infty = 1 + \chi_\infty$ , and the depolarization energy  $U_{dp}$  for the  $A_{2u}(\text{LO}_1)$  mode. In order to obtain insightful knowledge, we also plot in Fig. 5 each quantity obtained for  $A_{2u}(\text{TO}_1)$  (the TO mode) on the same figure so that a direct comparison can be made. Fig. 5(a) reveals that the well depth of the internal energy for  $A_{2u}(\text{TO}_1)$ ,  $-227$  meV, is indeed much deeper than the value of  $-13$  meV for  $A_{2u}(\text{LO}_1)$ ; the latter is barely noticeable in the inset of Fig. 5(a).

Interestingly, Fig. 5(b) reveals that the electric polarizations along the  $A_{2u}(\text{LO}_1)$  path and along the  $A_{2u}(\text{TO}_1)$  path exhibit drastic differences. Along the  $A_{2u}(\text{TO}_1)$  path, polarization rises rapidly from  $P = 0$

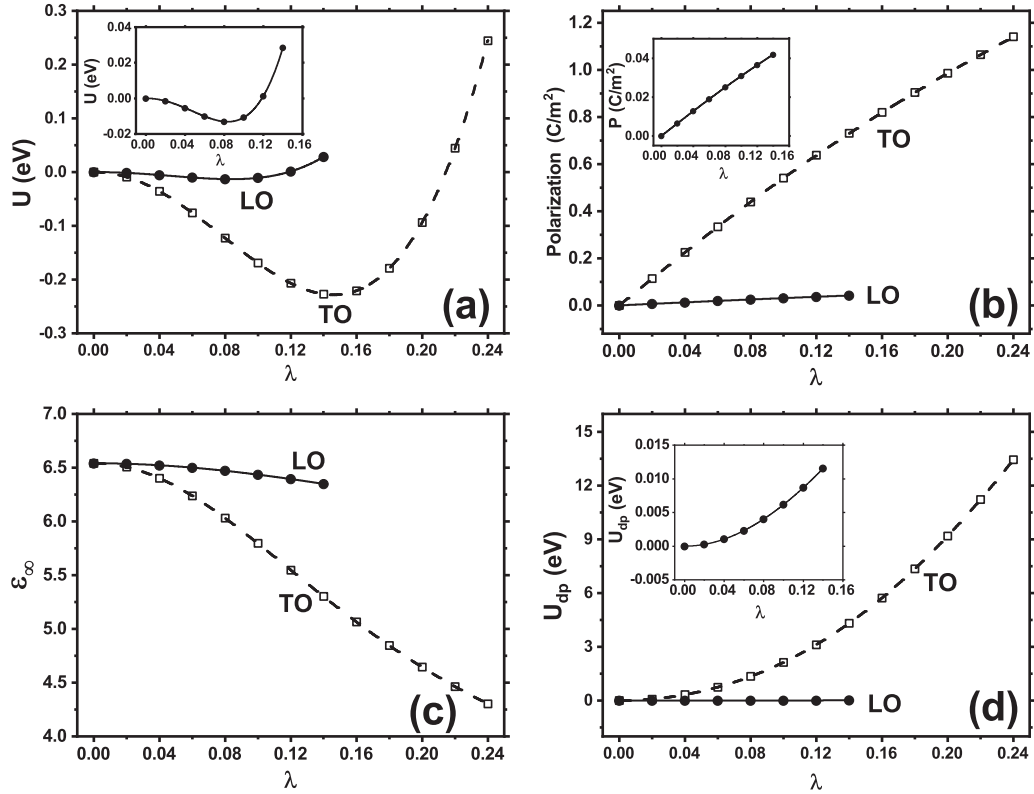


FIG. 5. Variations of the following quantities as a function of  $\lambda$ , for the  $A_{2u}(\text{LO}_1)$  mode (solid circles and labeled as LO) and for the  $A_{2u}(\text{TO}_1)$  mode (open squares and labeled as TO): (a) internal energy  $U(\lambda)$ , (b) polarization  $P(\lambda)$ , (c) high-frequency dielectric constant  $\epsilon_\infty(\lambda) = 1 + \chi_\infty(\lambda)$ , and (d) the depolarization energy  $U_{\text{dp}}$ . The insets in [(a)–(d)] are the blowup of the  $A_{2u}(\text{LO}_1)$  curve on small scale.

at  $\lambda = 0$  to  $P = 0.730 \text{ C/m}^2$  at  $\lambda = 0.14$  (which is near the internal-energy minimum of this TO mode). However, along the  $A_{2u}(\text{LO}_1)$  path, polarization increases very slowly from  $P = 0$  at  $\lambda = 0$  to merely  $P = 0.025 \text{ C/m}^2$  at  $\lambda = 0.08$  (which is near the internal-energy minimum of this LO mode). Quantitatively, the slope  $\frac{dP}{d\lambda} = 0.31 \text{ C/m}^2$  along the LO path is more than *one order of magnitude smaller* than the slope  $\frac{dP}{d\lambda} = 5.21 \text{ C/m}^2$  along the TO path, which is phenomenal.

We find that the key mechanism—by which  $A_{2u}(\text{LO}_1)$  is able to generate a free-energy minimum at nonzero  $\lambda$  (and thus HyFE)—originates from the small depolarization energy  $U_{\text{dp}}$ , as depicted in Fig. 5(d). From the inset of Fig. 5(d), we see that, at  $\lambda = 0.08$ , which is near the internal-energy minimum along the  $A_{2u}(\text{LO}_1)$  path, the depolarization energy  $U_{\text{dp}}$  is only 4 meV, which is remarkably small. Since  $U$  is  $-13 \text{ meV}$  at  $\lambda = 0.08$ , the free energy  $F = U + U_{\text{dp}}$  is still *negative* at this nonzero  $\lambda$  as shown in Fig. 3(a), allowing the existence of structure instability (and thus HyFE) for  $A_{2u}(\text{LO}_1)$  under OCBC. In contrast, along the  $A_{2u}(\text{TO}_1)$  path, at  $\lambda = 0.14$  near the internal-energy minimum of this path, the depolarization energy in Fig. 5(d) is 4.32 eV, far exceeding the internal-energy gain of  $-0.227 \text{ eV}$ . As a consequence, the free energy in Fig. 3(b) is positive when  $\lambda$  deviates from 0, and no structural instability occurs under OCBC along the  $A_{2u}(\text{TO}_1)$  path.

It is not surprising that the depolarization energy  $U_{\text{dp}}$  is small along the  $A_{2u}(\text{LO}_1)$  path, since  $U_{\text{dp}}$  is proportional to  $P^2$  and inversely proportional to  $\epsilon_\infty = 1 + \chi_\infty$  according to

Eq. (7). Our finding that the polarization increases slowly along the  $A_{2u}(\text{LO}_1)$  path [Fig. 5(b)] naturally leads to a small depolarization energy. The relatively larger  $\epsilon_\infty$  dielectric constant along the  $A_{2u}(\text{LO}_1)$  path [Fig. 5(c)], as compared to that along the  $A_{2u}(\text{TO}_1)$  path, further contributes to the small depolarization energy of  $A_{2u}(\text{LO}_1)$ .

#### D. Possible key quantity in the search for new HyFE

Another interesting and technologically-important question centers on whether there is any key physical quantity, which may help in the searching or designing of new hyperferroelectric solids. We find that such a quantity indeed exists, and it is the mode-specific effective charge (MEC),  $\tilde{Z}_\alpha^{n\vec{q}}$ , of a given phonon (not the effective charges of ions). Consider a phonon mode  $n\vec{q}$  with normalized eigendisplacement  $u_{i\beta}^{n\vec{q}}$ , the mode-specific effective charge  $\tilde{Z}_\alpha^{n\vec{q}}$  of this phonon is defined as

$$\tilde{Z}_\alpha^{n\vec{q}} = \sum_{i\beta} Z_{i,\alpha\beta}^* u_{i\beta}^{n\vec{q}}, \quad (8)$$

where  $Z_{i,\alpha\beta}^*$  is the dynamic Born effective charge of atom  $i$ ,  $n$  the phonon-branch index,  $\vec{q}$  the phonon wave vector, and  $\alpha$  and  $\beta$  the indices of Cartesian directions. Note that (i)  $\tilde{Z}_\alpha^{n\vec{q}}$  is a vector (not a tensor); (ii)  $\tilde{Z}_\alpha^{n\vec{q}}$  depends critically on phonon displacement  $u_{i\beta}^{n\vec{q}}$ . Using the definition in Eq. (8), the change in polarization for the atomic configuration constructed along the vibration direction of the  $n\vec{q}$  phonon will be  $\Delta P_\alpha = \frac{1}{\Omega} \tilde{Z}_\alpha^{n\vec{q}} a_0 \Delta\lambda$ , where  $a_0$  is the lattice constant. Note that

$\Delta P_\alpha$  is directly proportional to the mode-specific effective charge  $\tilde{Z}_\alpha^{nq}$ , not the Born effective charges  $Z^*$  of ions per se.

We compute the MEC along the polarization direction, namely  $\tilde{Z}_3$ , for the  $A_{2u}(\text{TO}_1)$  and  $A_{2u}(\text{LO}_1)$  modes, and the results are given in the fourth column of Table I. The  $\tilde{Z}_3$  value of  $A_{2u}(\text{TO}_1)$  is found to be 6.65, which is large and leads to the rapid increase of polarization in Fig. 5(b) for this TO mode as  $\lambda$  increases. Interestingly, and in sharp contrast, the  $\tilde{Z}_3$  value of  $A_{2u}(\text{LO}_1)$  is only 0.39, which is outstandingly small. This tiny MEC is critical in terms of giving rise to the very slow increase in the polarization when  $\lambda$  increases, as shown in Fig. 5(b) for the LO mode. Therefore, we find that MEC is likely a possible key quantity that is responsible for the small polarization, small depolarization energy  $U_{\text{dp}}$ , and the existence of HyFE. Meanwhile, we would also like to point out that, although our study of  $\text{LiNbO}_3$  suggests that small mode-specific effective charge is vitally important for the existence of HyFE, it nevertheless requires more studies on other hyperferroelectric solids to find out whether the conclusion can be generalized to other materials.

We recognize that  $\tilde{Z}_3 = 0.39$  of  $A_{2u}(\text{LO}_1)$  is even smaller than  $Z_{33}^* = 1.11$  of Li atom. This is rather interesting and meanwhile puzzling since (i) if  $A_{2u}(\text{LO}_1)$  involves only Li atoms alone, its  $\tilde{Z}_3$  value will be 1.11, which is still considerably larger than 0.39; (ii)  $Z_{33}^* = 9.03$  of Nb atoms and  $Z_{33}^* = -3.36$  of O atoms are (much) larger in magnitude than that of Li. The origin of the exceptionally small  $\tilde{Z}_3$  of  $A_{2u}(\text{LO}_1)$  can be intuitively understood by examining the phonon eigenvector of this mode in Fig. 2(c). Figure 2(c) shows that, although  $A_{2u}(\text{LO}_1)$  consists of a large amplitude from Li atoms, the contribution from Nb atoms cannot be neglected, however. Furthermore, note that Nb atoms vibrate along the *opposite* direction as Li atoms, and since  $Z_{33}^*$  of Nb is very large, a small vibration amplitude of Nb atoms will cancel, to a large extent, the contribution from Li atoms in Eq. (8), which leads to a small  $\tilde{Z}_3$  for  $A_{2u}(\text{LO}_1)$ .

### E. Existence of tristable states

The existence of soft LO mode has been previously used as a key benchmark for determining whether or not a solid is HyFE [1–3,14]. Is this benchmark always valid? Is it possible that the ground state may turn out to be non-HyFE even if a soft LO mode exists under OCBC? Since this is a subject of critical importance, we address it here.

As we report in the lower part of Table I, besides the soft  $A_{2u}(\text{LO}_1)$  mode, there exists another soft  $A_{2g}$  mode when  $C^{na}$  is included (i.e., under OCBC). Fig. 2(d) shows that, in  $A_{2g}$  mode, two Li atoms exhibit opposite displacements along the polar axis with respect to the central Nb atom; therefore the mode is nonpolar. Also note that under OCBC, the frequency of the  $A_{2g}$  mode,  $120i \text{ cm}^{-1}$ , is more unstable than the soft  $A_{2u}(\text{LO}_1)$  mode. It will be inappropriate to ignore the soft nonpolar  $A_{2g}$  mode and conclude  $\text{LiNbO}_3$  is a bistable HyFE. One key question is to determine how the soft  $A_{2g}$  mode may affect HyFE in  $\text{LiNbO}_3$  under OCBC.

We calculate the electric free energies for the configurations generated according to the phonon eigendisplacement of the  $A_{2g}$  mode, and the result is shown in Fig. 6(a). Since the  $A_{2g}$  mode is nonpolar, the depolarization energy  $U_{\text{dp}}$  is

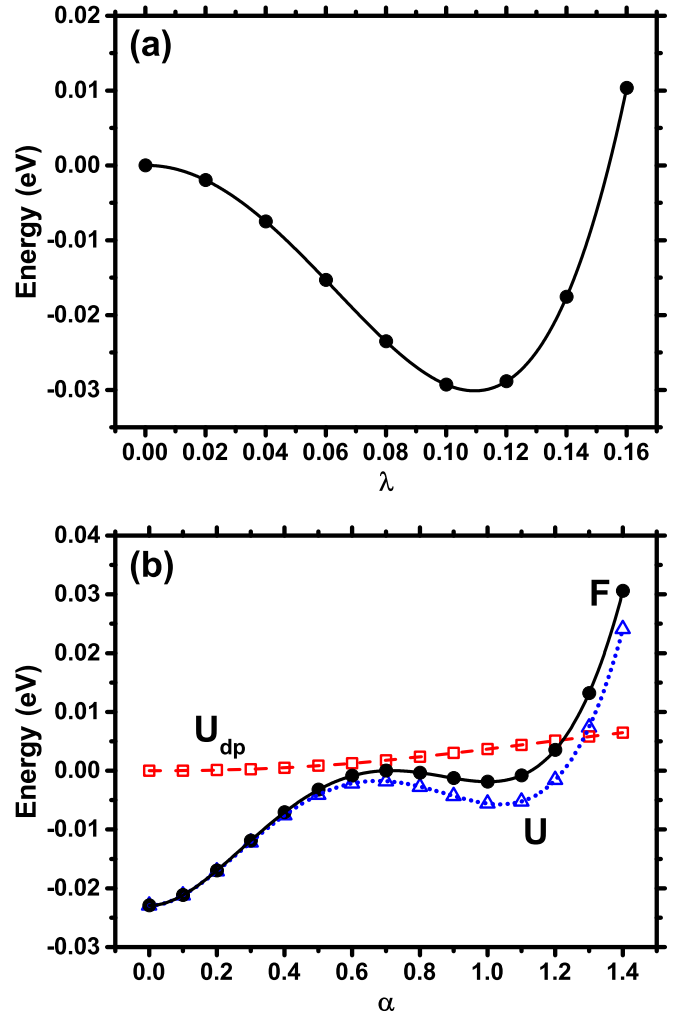


FIG. 6. Electric free energy  $F$  of  $\text{LiNbO}_3$  under OCBC for (a) the configurations generated according to the eigendisplacement of the soft  $A_{2g}$  mode, and (b) the configurations along the transition path from the nonpolar nP phase to the LO phase, where the internal energy  $U$  and the depolarization energy  $U_{\text{dp}}$  are also shown. In (a), internal energy is the only contribution to the free energy, and the depth of the potential well is  $-30.2 \text{ meV}$ . In (b), free energy  $F$  exhibits three local minima located at  $\alpha = 0$  and  $\alpha = \pm 1$ .

zero and the internal energy is the only contribution to the free energy under OCBC. Fig. 6(a) reveals that, when the free energy is at its minimum, the optimal  $\lambda$  value is 0.11. We name the configuration at this optimal  $\lambda$  as the nonpolar “nP” phase, and denote the configuration as  $\{\bar{r}_i^{\text{nP}}\}$ . Fig. 6(a) also tells us that the free-energy well depth of the nP phase is  $-30.2 \text{ meV}$ , which is about 3 times deeper than the counterpart of the  $A_{2u}(\text{LO}_1)$ -induced LO phase [see Fig. 3(a)]. Therefore, our calculations reveal that the ground state of  $\text{LiNbO}_3$  under OCBC is nonpolar, which is energetically more stable than the hyperferroelectric LO phase under OCBC. Importantly, the result also demonstrates that the existence of soft LO mode does not guarantee the occurrence of HyFE. One must be cautious when using the existence of soft LO mode as the hallmark criterion to determine whether a solid is HyFE.



It is interesting to point out that LiNbO<sub>3</sub> behaves rather differently from the hexagonal ABC-type semiconductor FEs such as LiBeSb and LiZnAs. Unlike the ABC-type semiconductor FEs in which only one soft LO phonon exists in the long-wavelength limit under OCBC [1], LiNbO<sub>3</sub> under OCBC exhibits a soft, nonpolar A<sub>2g</sub> mode in addition to a soft LO mode. Previous study focused only on the soft LO mode in LiNbO<sub>3</sub> and did not consider the nonpolar A<sub>2g</sub> mode, which inappropriately concluded that LiNbO<sub>3</sub> is HyFE [3].

After having established that the ground state of LiNbO<sub>3</sub> under OCBC is nonpolar, we further discover another intriguing possibility, that is, LiNbO<sub>3</sub> under OCBC exhibits unusual tristable states. To show this, we consider the configurations along the path connecting the nP phase and the LO phase, namely we examine the intermediate configurations according to  $\vec{r}_i(\alpha) = \vec{r}_i^{\text{nP}} + \alpha(\vec{r}_i^{\text{LO}} - \vec{r}_i^{\text{nP}})$ , where  $\vec{r}_i^{\text{nP}}$  and  $\vec{r}_i^{\text{LO}}$  are, respectively, the atomic positions of the nP and LO phases. Obviously,  $\alpha = 0$  and  $\alpha = 1$  correspond to the nP phase and LO phase, respectively. The calculated free energy is plotted in Fig. 6(b) as a function of parameter  $\alpha$ . We set the local maximum of the free energy between the nP and LO phases as the zero energy in Fig. 6(b).

Interestingly, Fig. 6(b) reveals that, in addition to the global minimum at  $\alpha = 0$ , there is one local free-energy minimum located at  $\alpha = 1$  (also at  $\alpha = -1$  due to symmetry), which is the hyperferroelectric LO phase with polarization  $P = 0.023$  C/m<sup>2</sup>. We also find that, with respect to the local maximum at  $\alpha = 0.7$ , the well depth of the free energy for the LO and nP phases are  $-1.9$  meV and  $-23$  meV, respectively. Therefore, we find that LiNbO<sub>3</sub> under OCBC possesses interesting tristable states (i.e., three local minima at  $\alpha = 0$  and  $\alpha = \pm 1$ ).

The finding—that LiNbO<sub>3</sub> transforms from polarization bistable states to tristable states when the boundary condition changes from SCBC to OCBC—is interesting in the following sense: (i) Unlike bistable states where the centrosymmetric state is unstable and cannot be accessed below the Curie temperature, the centrosymmetric nP phase in LiNbO<sub>3</sub> under OCBC is stable and can be accessed in experiments. (ii) As an unusual feature of the tristable states, the hysteresis loop in LiNbO<sub>3</sub> under OCBC will be different from the normal hysteresis of bistable states, by exhibiting the existence of a threshold electric field, which is required to move the system out of the stable centrosymmetric nP phase. This may also reduce the dielectric loss during the hysteresis [46]. (iii) The existence of tristable states can be technologically very useful by utilizing HyFE to design new FE applications such as ternary memory devices and on/off switching devices.

#### IV. CONCLUSIONS

We have employed a combination of linear-response perturbation theory, the modern theory of polarization, and electric free energy to investigate the hyperferroelectric properties of technologically important LiNbO<sub>3</sub> solid under OCBC. Our specific findings are summarized in the following.

(i) The longitudinal A<sub>2u</sub>(LO<sub>1</sub>) mode is soft with an imaginary frequency of  $96i$  cm<sup>-1</sup> in centrosymmetric LiNbO<sub>3</sub> under OCBC. Although the well depth of the *internal* energy is shallow and merely  $-13$  meV for the A<sub>2u</sub>(LO<sub>1</sub>) mode, we

find that this LO mode can nevertheless induce a free-energy minimum at nonzero polarization  $P=0.023$  C/m<sup>2</sup> (thus HyFE) under OCBC. The (HyFE) free-energy well depth is determined to be  $-9$  meV, which is comparable to the well depth of bulk BaTiO<sub>3</sub> under SCBC.

In contrast, the transverse A<sub>2u</sub>(TO<sub>1</sub>) mode, despite that it generates a very deep internal-energy well depth of  $-227$  meV, is found incapable of inducing HyFE under OCBC.

(ii) The origin why soft A<sub>2u</sub>(LO<sub>1</sub>) is able to generate a nonzero polarization under OCBC is revealed, and is found to result from the extraordinarily small depolarization energy, which is only  $+4$  meV. Combined with the (albeit small) internal-energy well depth of  $-13$  meV, the electric free energy still exhibits a minimum at nonzero polarization and thus HyFE under OCBC.

(iii) We further reveal that the soft A<sub>2u</sub>(LO<sub>1</sub>) mode is formed by the coupling between the soft A<sub>2u</sub>(TO<sub>1</sub>) mode and *nonsoft* A<sub>2u</sub>(TO<sub>2</sub>) mode, and a large majority contribution of 61% comes from the nonsoft A<sub>2u</sub>(TO<sub>2</sub>). Our study thus shows knowledge that nonsoft mode may play a pivotal role in developing HyFE.

(iv) We find a critical physical quantity that is important in the searching and designing of new HyFE materials, and the quantity is the mode-specific effective charge  $\tilde{Z}_\alpha^{nq}$  defined in Eq. (8). We further determine that  $\tilde{Z}_3^{nq}$  is very small and merely 0.39 for A<sub>2u</sub>(LO<sub>1</sub>) in LiNbO<sub>3</sub>, which is 1700% smaller than  $\tilde{Z}_3^{nq} = 6.65$  for A<sub>2u</sub>(TO<sub>1</sub>). In fact,  $\tilde{Z}_\alpha^{nq}$  can in principle approach zero for LO modes. A tiny  $\tilde{Z}_\alpha^{nq}$  gives rise to a very small depolarization energy  $U_{\text{dp}}$  and thus HyFE under OCBC.

(v) Despite that A<sub>2u</sub>(LO<sub>1</sub>) can induce HyFE, we discover that the ground state of LiNbO<sub>3</sub> under OCBC is nevertheless not HyFE. The reason that the ground state of LiNbO<sub>3</sub> is not HyFE is caused by the fact that, in addition to soft A<sub>2u</sub>(LO<sub>1</sub>), there exists another soft nonpolar A<sub>2g</sub> mode in LiNbO<sub>3</sub> under OCBC, which dominates the structure distortion and produces a nonpolar ground state. Our calculations thus reveal that the existence of a soft LO mode does not guarantee that the solid will be HyFE. One need be cautious in using this criterion to determine HyFE.

(vi) We further reveal an intriguing possibility that LiNbO<sub>3</sub> is tristable under OCBC. More specifically, we find that, along the configuration path transitioning from the ground-state nonpolar nP phase to the polar LO phase, LiNbO<sub>3</sub> under OCBC possesses three stable polarization states, which are located at  $P = \pm 0.023$  and  $0$  C/m<sup>2</sup>. The free-energy potential wells for the nP and LO phases are calculated to be  $-23$  meV and  $-1.9$  meV, respectively. The finding of tristable states in LiNbO<sub>3</sub> under OCBC may open phenomena and possibilities of technological applications. We hope the rich and interesting results in this paper will stimulate more theoretical and experimental interest on hyperferroelectricity.

#### ACKNOWLEDGMENTS

Computations were performed on the computing facilities provided by the Arkansas High-Performance Computing Center, supported by National Science Foundation.

- [1] K. F. Garrity, K. M. Rabe, and D. Vanderbilt, *Phys. Rev. Lett.* **112**, 127601 (2014).
- [2] H. Fu, *J. Appl. Phys.* **116**, 164104 (2014).
- [3] P. Li, X. Ren, G.-C. Guo, and L. He, *Sci. Rep.* **6**, 34085 (2016).
- [4] C. J. Fennie and K. M. Rabe, *Phys. Rev. B* **72**, 100103(R) (2005).
- [5] E. Bousquet, M. Dawber, N. Stucki, C. Lichtensteiger, P. Hermet, S. Gariglio, J.-M. Triscone, and P. Ghosez, *Nature (London)* **452**, 732 (2008).
- [6] N. A. Benedek and C. J. Fennie, *Phys. Rev. Lett.* **106**, 107204 (2011).
- [7] M. Dawber, K. M. Rabe, and J. F. Scott, *Rev. Mod. Phys.* **77**, 1083 (2005).
- [8] J. Junquera and P. Ghosez, *Nature (London)* **422**, 506 (2003).
- [9] N. A. Benedek and M. Stengel, *Physics* **7**, 32 (2014).
- [10] S. Liu and R. E. Cohen, *Phys. Rev. Lett.* **119**, 207601 (2017).
- [11] M. E. Lines and A. M. Glass, *Principles and Applications of Ferroelectrics and Related Materials* (Clarendon Press, Oxford, 1977).
- [12] J. F. Scott and C. A. Paz de Araujo, *Science* **246**, 1400 (1989).
- [13] J. F. Scott, *Ferroelectric Memories* (Springer, Berlin, 2000).
- [14] M. Khedidji, D. Amoroso, and H. Djani, *Phys. Rev. B* **103**, 014116 (2021).
- [15] H. J. Zhao, A. Filippetti, C. Escorihuela-Sayalero, P. Delugas, E. Canadell, L. Bellaiche, V. Fiorentini, and J. Iniguez, *Phys. Rev. B* **97**, 054107 (2018).
- [16] R. S. Weis and T. K. Gaylord, *Appl. Phys. A* **37**, 191 (1985).
- [17] M. R. Chowdhury, G. E. Peckham, and D. H. Saunderson, *J. Phys. C: Solid State Phys.* **11**, 1671 (1978).
- [18] W. G. Schmidt, M. Albrecht, S. Wippermann, S. Blankenburg, E. Rauls, F. Fuchs, C. Rodl, J. Furthmuller, and A. Hermann, *Phys. Rev. B* **77**, 035106 (2008).
- [19] S. Sanna, S. Neufeld, M. Rusing, G. Berth, A. Zrenner, and W. G. Schmidt, *Phys. Rev. B* **91**, 224302 (2015).
- [20] S. Margueron, A. Bartaszyte, A. M. Glazer, E. Simon, J. Hlinka, I. Gregora, and J. Gleize, *J. Appl. Phys.* **111**, 104105 (2012).
- [21] M. Friedrich, A. Schindlmayr, W. G. Schmidt, and S. Sanna, *Phys. Status Solidi B* **253**, 683 (2016).
- [22] S. Sanna, G. Berth, W. Hahn, A. Widhalm, A. Zrenner, and W. G. Schmidt, *Ferroelectrics* **419**, 1 (2011).
- [23] S. Baroni, S. Gironcoli, A. D. Corso, and P. Giannozzi, *Rev. Mod. Phys.* **73**, 515 (2001).
- [24] S. Baroni, P. Giannozzi, and A. Testa, *Phys. Rev. Lett.* **58**, 1861 (1987).
- [25] X. Gonze, *Phys. Rev. A* **52**, 1096 (1995).
- [26] X. Gonze and C. Lee, *Phys. Rev. B* **55**, 10355 (1997).
- [27] D. M. Eagles, *J. Phys. Chem. Solids* **25**, 1243 (1964).
- [28] W. Zhong, R. D. King-Smith, and D. Vanderbilt, *Phys. Rev. Lett.* **72**, 3618 (1994).
- [29] A. Raeliarijaona, and H. Fu, *Phys. Rev. B* **92**, 094303 (2015).
- [30] R. D. King-Smith and D. Vanderbilt, *Phys. Rev. B* **47**, 1651 (1993).
- [31] R. Resta, *Rev. Mod. Phys.* **66**, 899 (1994).
- [32] R. Adhikari and H. Fu, *Phys. Rev. B* **99**, 104101 (2019).
- [33] M. Born and K. Huang, *Dynamical Theory of Crystal Lattices* (Clarendon Press, Oxford, 1988).
- [34] Y. Yao and H. Fu, *Phys. Rev. B* **79**, 014103 (2009).
- [35] M. Stengel, N. A. Spaldin, and D. Vanderbilt, *Nat. Phys.* **5**, 304 (2009).
- [36] P. Giannozzi, S. Baroni, N. Bonini, M. Calandra, R. Car, C. Cavazzoni, D. Ceresoli, G. L. Chiarotti, M. Cococcioni, I. Dabo *et al.* *J. Phys.: Condens. Matter* **21**, 395502 (2009).
- [37] See, <https://www.quantum-espresso.org>.
- [38] N. Troullier and J. L. Martins, *Phys. Rev. B* **43**, 1993 (1991).
- [39] S. C. Abrahams, J. M. Reddy, and J. L. Bernstein, *J. Chem. Phys. Solids* **27**, 997 (1966).
- [40] S. H. Wemple, M. DiDomenico Jr., and I. Camlibel, *Appl. Phys. Lett.* **12**, 209 (1968).
- [41] M. Ye and D. Vanderbilt, *Phys. Rev. B* **93**, 134303 (2016).
- [42] A. V. Postnikov, V. Caciuc, and G. Borstel, *J. Phys. Chem. Solids* **61**, 295 (2000).
- [43] M. Veithen and P. Ghosez, *Phys. Rev. B* **65**, 214302 (2002).
- [44] Our calculated frequency  $202i\text{ cm}^{-1}$  for  $A_{2u}(\text{TO}_1)$  agrees well with  $201i\text{ cm}^{-1}$  in Ref. [43] and with  $183i\text{ cm}^{-1}$  in Ref. [18].
- [45] H. Fu and R. E. Cohen, *Nature (London)* **403**, 281 (2000).
- [46] A. D. L. Chandani, T. Hagiwara, and Y. Suzuki, *Jpn. J. Appl. Phys.* **27**, L729 (1988).